CrossMark

Hydrodynamically efficient micropropulsion through a new artificial cilia beating concept

Yu-An Wu[1] · Bivas Panigrahi[1] · Chia-Yuan Chen[1]

Abstract Flow propulsion and manipulation in a microscale flow regime are essential for the rapid processing of biomedical analytical assays that are performed on lab-on-a-chip platform. However, inherited from typically conical movement of artificial cilia in a cyclic manner, the generated backflow and flow oscillations during artificial cilia actuation are inevitably significant and post a significant barrier to the practical use of artificial cilia for accurate flow control. To address this problem, in this study we have hypothesized that by minimizing the traversing path of the artificial cilia during the recovery stroke could minimize the generated back flow and will result in an increment in the net flow propulsion. In this aspect, we have initiated the concept of the triangular beating pattern and compared its performance with the typical circular beating pattern. Upon comparison, it was observed that in the case of triangular beating pattern, the generated peak net flow velocity is almost double than the case of circular beating pattern. In particular, the underlying hydrodynamics induced during the actuation of the aforementioned two distinct beating patterns of artificial cilia were visualized and quantified with delineated comparison. This comparison was conducted based on flow dynamic characteristics measured through a micro-particle image velocimetry method. These results are important given that previous researchers do not explicitly recognize the role of the triangular beating pattern which possesses a significantly hydrodynamic advantage that can reduce the amount of back flow and surrounding flow fluctuations. The proposed concept provides a novel perspective on the microscale flow manipulation with promising applications in micropropulsion.

1 Introduction

Microscale flow propulsion is responsible for generating temporal and volumetric fluid movements to accurately and reliably transport a fluidic sample (e.g., drugs and therapeutic agents) from a reservoir to the target on a lab-on-a-chip. This method is critical to the overall efficiency of the miniaturized device for various biomedical, pharmaceutical, and even environmental monitoring applications. Several examples can be found in other fields (Abhari et al. 2012). Previously reported flow pumping mechanisms can be classified into two categories, namely, mechanical and non-mechanical micropumps. The former requires a physical actuator to propel the fluid, whereas the latter requires energy transformation from non-mechanical energy to kinetic momentum of fluid elements to drive the flow (Laser and Santiago 2004). Possible interferences or reactions may occur between the flow-transporting mediums and biological samples that are transported within the non-mechanical micropumps. Hence, the mechanical type is considerably favorable in most micro total analysis systems with the actuator that is often highly inert to biomolecules and buffers (Vilfan et al. 2010). Therefore, identifying a reliable and robust micromanipulator for highly accurate flow generation can be beneficial.

Nature provides an ingenious solution to the aforementioned need by means of long elastic filaments called cilia. These hair-like structures beat in a whip-like and conical manner, which comprises effective and recovery strokes with asymmetrical beating patterns (Gauger et al. 2009). Effective stroke is made by pivoting from the base of the

✉ Chia-Yuan Chen
  chiayuac@mail.ncku.edu.tw

1 Department of Mechanical Engineering, National Cheng Kung University, No. 1 University Road, Tainan 701, Taiwan

cilium. The cilium itself remains relatively straight and rigid during this phase. However, the cilium is allowed to relax along its length during the recovery stroke. Consequently, the recovery stroke induces less resistance than the power stroke; hence, an organism is able to use the cilia for locomotion by dragging fluid over its surface (Dorin and Martin 1994). Apart from this asymmetry, natural cilia beat in a sequential manner, in which a phase lag between any two adjacent cilia is observed. This phenomenon is called metachronal waving, which works based on the direction difference between the propagating wave and the object's surface with cilia attached to it. Two types of metachronal rhythm, namely, antiplectic and symplectic metachronisms, are described when the directions between these rhythms are the same in the former and opposite in the latter (Toonder and Onck 2013). These motion characteristics constitute the efficient thrust force generation in the low Reynolds flow regime, which was recognized and detailed in the Scallop theorem (Purcell 1977).

A recent trend presents the use of engineering processes to design a cluster of flow manipulators, called artificial cilia, in a manner thatmimics the unique beating behaviors of natural cilia. These artificial cilia can be actuated with various applied external energy, including optical (Van Oosten et al. 2009), magnetic (Belardi et al. 2011; Chen et al. 2013; Evans et al. 2007; Gauger et al. 2009; Onck et al. 2011; Vilfan et al. 2010), and electrical (Den Toonder et al. 2008) forces. Considering the symmetric beating nature of artificial cilia, no propulsion should be generated in an artificial cilia based microfluidic device. However, a net propulsion was evidenced with this kind of device by positioning the artificial cilia near to one side of the micro channel wall. Detail discussion regarding this aspect can be found elsewhere (Chen et al. 2015). Similar concept had also been implemented in a bidirectional microfluidic system where net pumping was evidenced, through the symmetrically spinning rotation of ferromagnetic Janus microspheres around permalloy disks, actuated through an external magnetic field (Van den Beld et al. 2015). With this experimental setup a pumping of 0.3 nL/min could be generated. Apparently, in both these aforementioned micro propulsion systems, the rotating objects such as the artificial cilia and Janus microspheres placed close to one side of the microchannel wall so that asymmetry in the liquid displacement can be found in each symmetrically rotation cycle of rotating objects, resulting a net pumping inside the microchannel. Still, considering the amount of back flow generated during the recovery stroke of artificial cilia rotation, these devices generates highly oscillated flow field. For this study, it was hypothesized that by reducing the traversing path of the artificial cilia during the recovery stroke will significantly curtail the amount of back flow, hence

resulting an increment in the net flow generation. In this aspect, through this study a triangular beating pattern of artificial cilia is being proposed, where during the recovery stroke, the cilia traverse in a straight path with the specific objective to reduce the amount of back flow. A flow visualization scheme and parametric studies are presented in this study in an attempt to identify an improved flow propelling method to advance the efficiency of current lab-on-a-chip platforms.

2 Materials and methods

2.1 Fabrication of the artificial cilia based microchannel

Figure 1 shows a series of computerized numerical control (CNC) micromachining processes followed by polydimethylsiloxane (PDMS, Sylgard 184, Dow Corning Corp., Midland, USA) casting, which was adopted for the fabrication of the artificial cilia-based microchannel. Both the desired mold for the microchannel and artificial cilia were engraved onto a 5 mm thick acrylic substrate using a CNC micro-milling machine. The desired microchannel configuration was achieved through micro-milling and micro-drilling using two different drill bit types. A 800 μm bit was used during the micro-milling process, the specific objective of which was to engrave the microchannel geometric pattern on the substrate while achieving a smooth surface finish. Thereafter, micro-holes (50 μm diameter and 400 μm depth) were drilled on the substrate's surface using a 50 μm drill bit to engrave the mold for the artificial cilia. This aspect ratio (depth/diameter) of the artificial cilia was predetermined in our previously published article and designed to ensure a high degree of artificial cilia functionality (Chen et al. 2015).

To fabricate the artificial cilia, a composite that is a homogeneous mixture of commercially available 5 μm neodymium–iron–boron particles (MQP-15-7, Magnequench, Singapore) and PDMS solution in a weight ratio of 1:4 permeated into their respective mold. Subsequently, the entire mold was filled with degassed PDMS followed by a curing process through a hot plate baking at 95 °C for 48 h. After the stipulated time, the PDMS replica was peeled from the parent mold; each artificial cilium was magnetized to obtain actuation relative to the applied external magnetic field. Two holes corresponding to the inlet and outlet were drilled using a conventional drilling machine to introduce tubing's for fluid facilitation. Further, microchannel openings were sealed by treating them with oxygen plasma and bonding them using a microscopic cover slip.
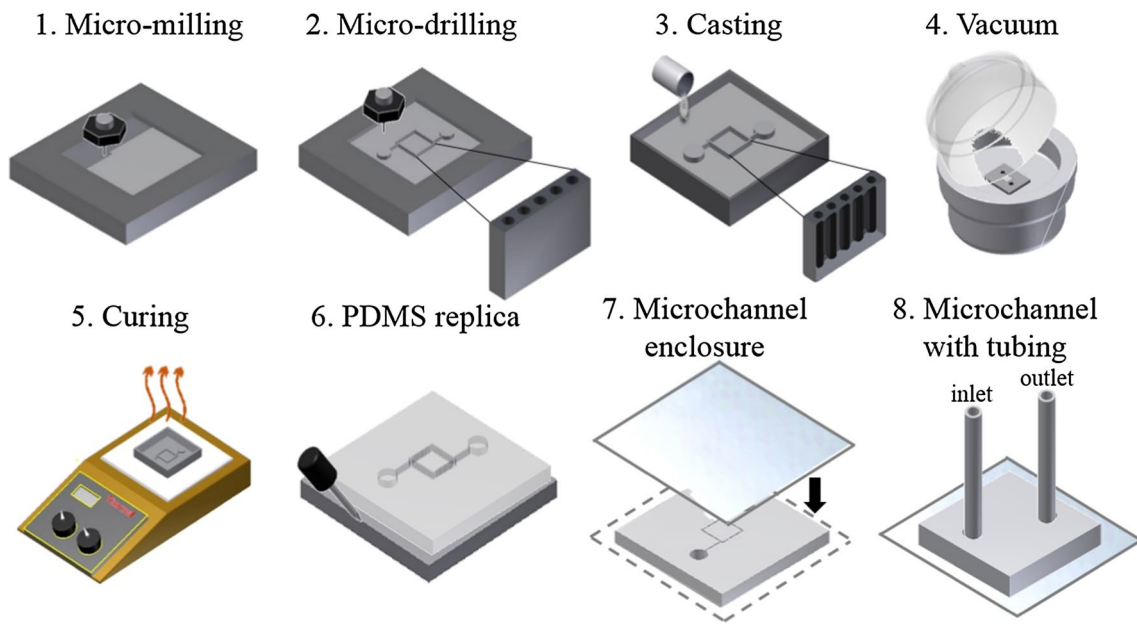
Fig. 1 Schematic depiction of the fabrication process of the artificial cilia embedded microchannel for flow propulsion

2.2 Design and manufacturing

The microchannel layout, which is schematically shown in Fig. 2a, was drafted using a computer-aided design environment. The microchannel was designed to embody two types of microchannel regions, namely, zones with and without artificial cilia. The zones with artificial cilia (i.e., Zones A and C) provided a propulsion to the matter
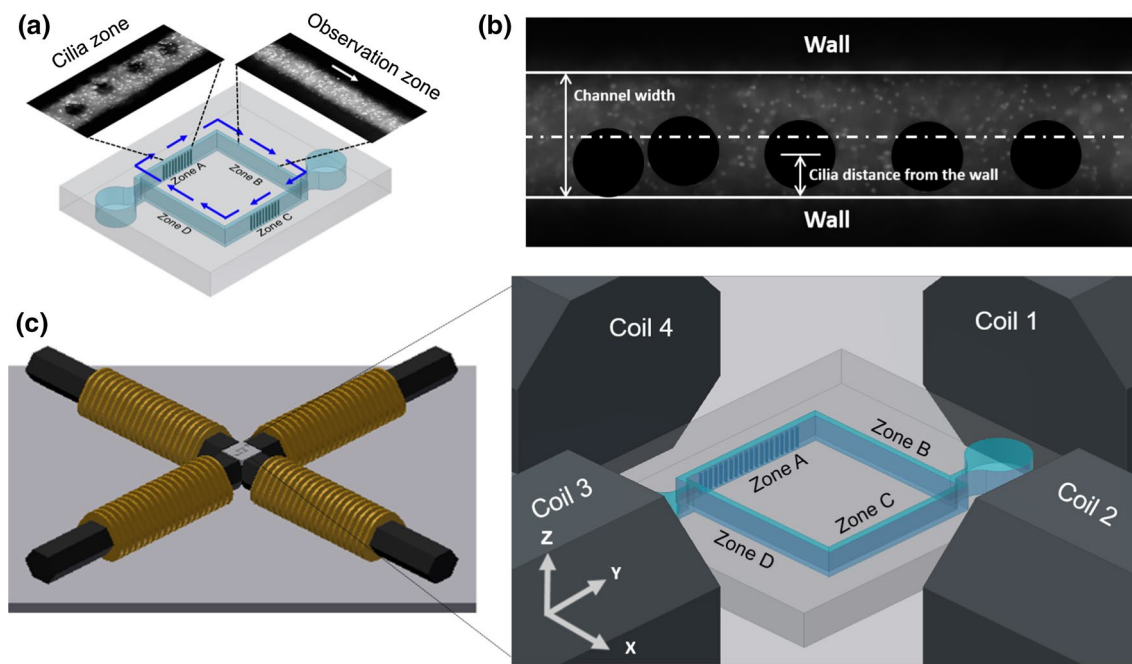

Fig. 2 a Schematic depiction of the microchannel illustrating the cilia and observation zones. **b** The *top view* of the fabricated microchannel with the embedded artificial cilia. Though the array of artificial cilia was designed in the center of the microchannel but during the microfabrication process, due to the effect of residual stress they lean towards one side of the microchannel wall that forms an asymmetry, further resulting some amount of propulsion with the circular beating pattern. **c** *Image* showing the relative orientation of the microchannel and the actuation system. Among the four zones, two zones namely Zones B and D were there to observe the fluid behaviors

of interest. The other two zones without artificial cilia (i.e., Zones B and D) were designed to observe the fluid behaviors and reserved for the analyses. This is designed in such a way that the biomechanical behavior of the biological species can be studied under varying flow stresses induced from the artificial cilia. Figure 2b illustrates the top view of the artificial cilia jutting out from the bottom of the microchannel. The array of artificial cilia was situated close to one side of the microchannel wall. The distance between the center points of each artificial cilium corresponding to the microchannel wall were quantified and it was evidenced, corresponding to the channel width of 90 μm, the artificial cilia were positioned at a distance of 39.26 ± 12.85 μm from the nearest microchannel wall. To study the artificial cilia population and their distribution toward the net flow propulsion, an experiment was designed and conducted in four distinctive modes (i.e., Modes I–IV). Relative orientation of the microchannel and artificial cilia actuation system has been illustrated in the Fig. 2c. Table 1 illustrates that Modes I and II were designed to identify the effects of the artificial cilia population on the generated net flow propulsion. The population distribution on the generated net flow propulsion was studied in Modes I, III, and IV by varying the number of artificial cilia in their respective zones.

2.3 Motion control of artificial cilia trajectory

An in-house magnetic actuation system was employed during the experiment to ensure a precise flow manipulation through artificial cilia motion. This system consists of four magnetic coils that are equally distributed on a horizontal plane, integrated data acquisition device (NI cDAQ-9174, National Instruments, Austin, TX) with output module (NI 9264), switching circuit, customized graphical user interface, and power supply (GPR-3510HD DC Power Supply, Instek, Taiwan). The data acquisition module was connected to the coils and external power supply via a switching circuit. Each individual magnetic coil was made by winding approximately 1200 turns of enameled 24 gauge magnetic wire on a hexagonal iron bar. Using external power, these magnets served as electromagnets; a magnetic field of up to 0.8 T could be generated through the magnetic actuation system. A modulated pulse width modulation (PWM) waveform with a switching frequency of 240 Hz (to reduce the effect of hysteresis) was used to manage the time duration of the power supply. It was observed that the scanning area (area under the trajectory traversed by the cilia tip) was inversely proportional to the magnitude of artificial cilia rotating frequency (data not provided). In lower frequency such as 10 Hz, actual radius of cilia trajectory supposed to be as high as 40 μm. However, due to narrow width of the microchannel, there was

Table 1 Distribution of the artificial cilia in their respective zones by varying their positions and number during the four experimental conditions (i.e., Modes 1 to 4)

Cilia Zone \ Mode	I	II	III	IV
A	20	10	15	10
B	0	0	0	0
C	0	0	5	10
D	0	0	0	0

a considerable effect of the microchannel wall and lateral displacement of the cilium trajectory got restrained. Contrast to this, at higher artificial cilia rotational frequency such 50 Hz, a defined circular trajectory of the artificial cilia tip was evidenced. However no flow could be generated with this setting. Therefore, to eliminate the interaction of the artificial cilia and microchannel wall along with a net flow generation, the rotational frequency of the artificial cilia was determined to 40 Hz.

The aforementioned experiment aimed to evaluate the influences of the circular and triangular artificial cilia trajectories (denoted as patterns I and II, respectively, in Fig. 3) on the net flow propulsion. In order to achieve both the desired artificial cilia beating patterns, each of the magnetic coil's duty cycle altered in a range of 0–100%, through two distinct motion control algorithms. In general, duty cycle refers to the relationship between the operating and the resting period of the switching circuit which supplies current to the magnetic coils. A larger duty cycle corresponds to a higher amount of current supply to the actuation system ensuring substantial magnetic field that confirms a larger tilting angle to the artificial cilia towards the direction of the larger magnetic field. The circular beating trajectory (addressed as Pattern I in the corresponding Fig. 3) of the artificial cilia was achieved by changing the duty cycle of the four magnetic coils in a time step of eight during a 3.125 ms time span through implementing the motion control algorithm which is in the form of sine and cosine relations along the x- and y-directions (listed in Eqs. 1 and 2).

$$Magnetic\ field(x) = -M_0 \cos\left(2\pi \cdot \frac{t}{T}\right) \tag{1}$$

$$Magnetic\ field(y) = M_0 \sin\left(2\pi \cdot \frac{t}{T}\right) \tag{2}$$

where M_0 is the base amplitude, t is the instantaneous time, and T indicates the total time period of a cycle. Towards achieving a triangular trajectory of artificial cilia, the duty
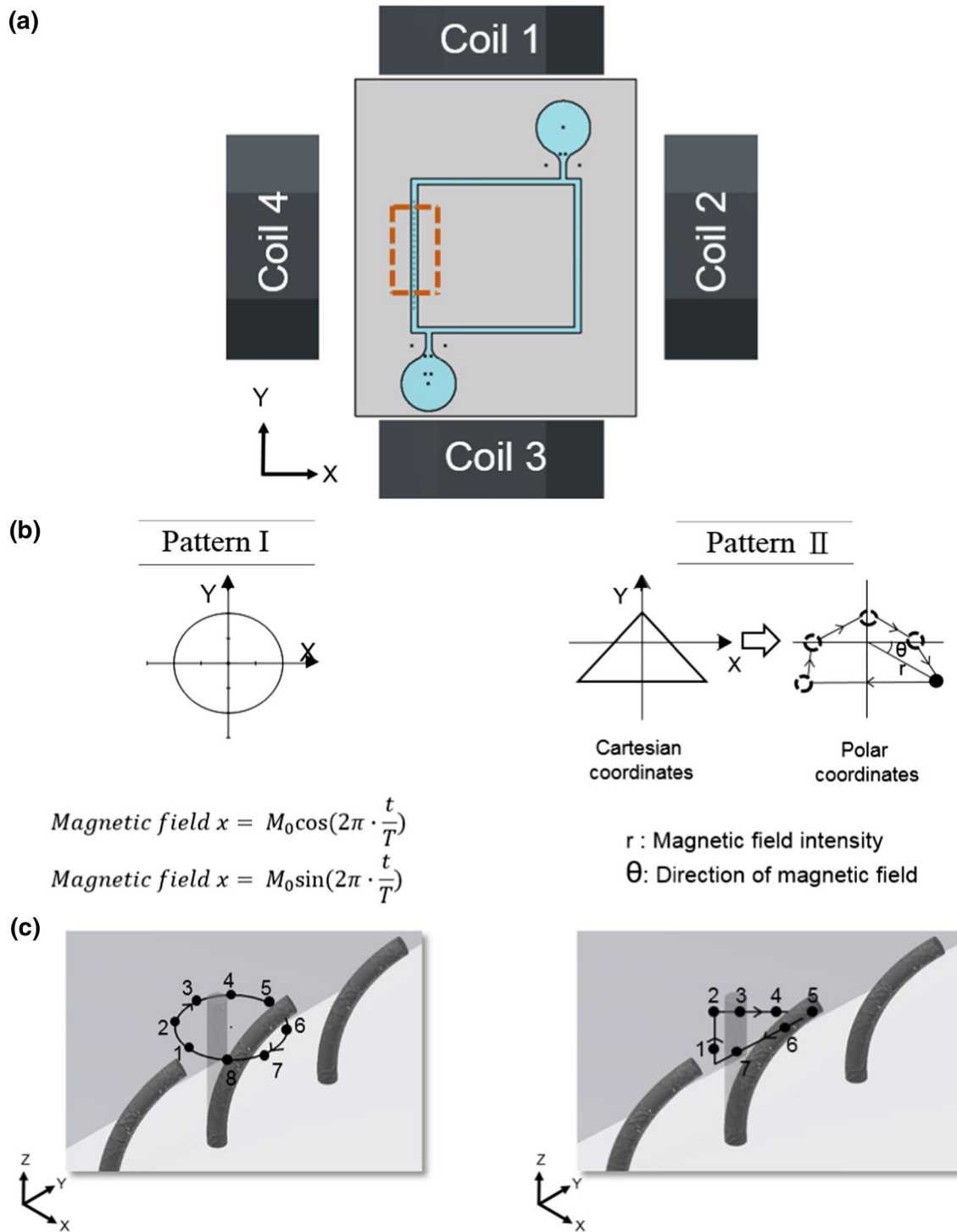
(a)

(b)

Pattern I

$$Magnetic\ field\ x\ =\ M_0\cos(2\pi\cdot\frac{t}{T})$$

$$Magnetic\ field\ x\ =\ M_0\sin(2\pi\cdot\frac{t}{T})$$

Pattern II

Cartesian coordinates

Polar coordinates

r : Magnetic field intensity
θ: Direction of magnetic field

(c)

Fig. 3 Illustrations of the two selected trajectories of artificial cilia to evaluate the influences of the artificial cilia beating behaviors on the net flow propulsion. **a** Schematic illustration of the orientation of the microchannel inside the magnetic actuation system (*yellow dashed box* illustrates the position of artificial cilia inside the microchannel), dimensions are not in scale. **b** Two beating patterns (denoted as patterns I and II) of the artificial cilia through the coordinate system. c Illustration of the 3D view of the artificial cilia trajectories

cycle of the four magnetic coils was altered in a time step of seven during a 3.571 ms time span (addressed as Pattern II in the corresponding Fig. 3) through trajectory recognition technique (Chen et al. 2014). To determine the traversing path of the artificial cilia, the locus of the premeditated Cartesian coordinates of a triangle (x_n, y_n, where n = 1–7) were

imported and further altered to the polar coordinate system by evaluating the base amplitude ($r = \sqrt{x_n^2 + y_n^2}$) and the direction of the magnetic field ($\theta = \tan^{-1} \frac{y_n}{x_n}$). Once the coordinates for the trajectory were identified, duty cycles of the four magnetic coils altered accordingly so that artificial cilia tip can traverse the desired actuation path.

2.4 Flow quantification through micro-particle image velocimetry (µPIV)

The µPIV method was used to quantify the generated flow propulsion in the proposed artificial cilia-based microchannel. To conduct the flow measurement experiment, 0.1–0.3% fluorescent micro particles of 3.2 µm diameter (Microgenics, Inc., Fremont, CA, USA) were induced in the microchannel using a syringe pump. A fluorescent microscope (BX60, Olympus Corp., Japan) was employed to quantify the particle motion with respect to time. Using this microscope, instantaneous flow at the observation zone in a plane consistent with the artificial cilia tip was imaged and processed by commercially available PIV software (proVISION, IDT, Tallahassee, FL, USA). To quantify the velocity, an adaptive interrogation method with a spatial resolution of 6 µm was used. The validity of this methodology had been demonstrated in various studies by matching the results from theoretical and experimental data (Chen et al. 2013). To delineate the flow generated through the proposed device, the flow field in the observation zone was recorded through a high speed camera at a frame rate of 200 Hz, meanwhile the artificial cilia rotating at a speed of 40 Hz. Corresponding to the observed oscillatory flow field at each artificial cilia rotational cycle, the

peak flow velocities recorded during the forward and backward stroke were coined as $V_{x,max}$ and $V_{x,min}$ meaning that both the maximum and minimum flow velocities in each flow domain were recorded. To facilitate the comparison of the generated velocity spatially and temporally in different modes, the measured velocity values are presented in the form of $V_{x,max}$ and $V_{x,min}$ where the peak values were collected and added up together in each measured flow domain at each given time step. Additionally, an in-house post-processing method was employed during the velocity calculation to reduce the effect of vibration caused by the magnetic coils in switching the applied current.

3 Results and discussion

3.1 Effect of artificial cilia population

Figure 4 describes the investigation of the effect of the number of artificial cilia to the generated flow velocity. Figure 4a shows that $V_{x,max} + V_{x,min}$ reached as high as 180.5 µm/s in Mode II, whereas the sum was merely 162.4 µm/s in Mode I. This difference indicated that an increase in the number of artificial cilia does not result in a direct increase in the flow that can be generated. This finding contradicts the original idea that an additional number of artificial cilia could lead to considerably substantial flow generation. Hence, the induced flow interaction encountered by two adjacent synchronized artificial cilia rotating in a circular manner may either strengthen or weaken the generated flow magnitude. This finding was further proven by the net flow comparison between these two modes, as
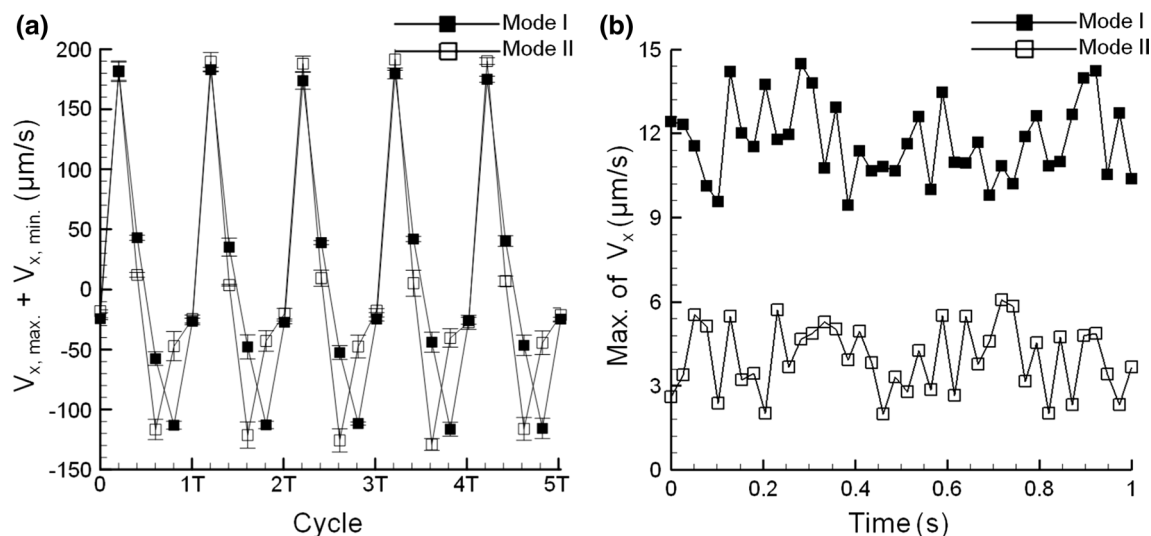

Fig. 4 Time-dependent generated flow velocity comparison between two sets of artificial cilia numbers quantified using µPIV at frame rates of 200 Hz (**a**) and 40 Hz (**b**). The artificial cilia are rotated by

following a circular trajectory at a rotational rate of 40 Hz. *Error bar* shows one standard deviation of the measured results over three cycles

shown in Fig. 4b. In this subfigure, the net flow was calculated in a condition in which the image capture rate was synchronized with the rotational frequency of the artificial cilia array. The average net flow velocity generated using Mode I over five cycles was measured at 11.7 µm/s with a 14.5 µm/s peak velocity. By contrast, the values generated in Mode II were nearly three times lower (4.0 µm/s) and twice lower, respectively, than those in Mode I. These results demonstrate the necessity of systematically investigate the flow phenomenon to identify the population and distribution of artificial cilia towards net flow generation. In a case where the number of artificial cilia is over 20 has yet to be considered as the total length of the artificial cilia array spanning along the axis in Zone A will exceed the coverage of the applied homogeneous magnetic field, thereby resulting in unsynchronized artificial cilia movement that potentially obstructs flow generation. Therefore, 20 artificial cilia were selected and arranged for follow-up analyses.

Theoretically, with cyclic trajectory of artificial cilia, no flow should be generated due to the symmetric pattern of motion during the effective and recovery stroke. However, in contrast to this theoretical fact, in our experiment a moderate flow was evidenced with the circular beating patterns which can be described by shedding light in the artificial cilia's orientation inside the microchannel where they positioned close to the microchannel wall. As artificial cilia travels close to the microchannel wall, its beating is rationally affected by the microchannel's wall during the recovery stroke further reducing the magnitude of the back flow. However, a substantial flow was generated during the effective stroke and corresponding to the lower magnitude flow during the recovery stroke, an overall net propulsion was evidenced in the respective direction of the effective stroke.

3.2 Effect of distribution of artificial cilia

The effect of artificial cilia distribution within the microchannel towards the net flow generation has been investigated in the preceding section. The flow generated by three different modes, namely, ModesI, III, and IV, with the same number of artificial cilia but variedly distributed in Zones A and C, were compared at two image acquisition rates (200 Hz in Fig. 5a and 40 Hz in Fig. 5b). In the Mode IV distribution, where 20 artificial cilia were distributed equally in Zones A and C, the largest amount of flow generation can be achieved among the three modes being compared. However, this condition comes with the highest flow oscillation that leads to significant flow fluctuations. The peak forward flow velocity reached 453.6 µm/s and was −233.6 µm/s for the peak backward flow velocity. Similar findings can be observed for the flow generated with Mode III distribution. Thus, substantial flows can be generated with the artificial cilia distributed in Zones A and C compared with the single zone distribution of artificial cilia in Mode I. In the case of the net flow comparison, Fig. 5b shows that the Mode I data exhibited the second highest net flow generation among the three modes. This finding identifies the effect of artificial cilia distribution in terms of flow generation with limited fluctuations. For ModesIII and IV distributions, the generated flow is noteworthy but
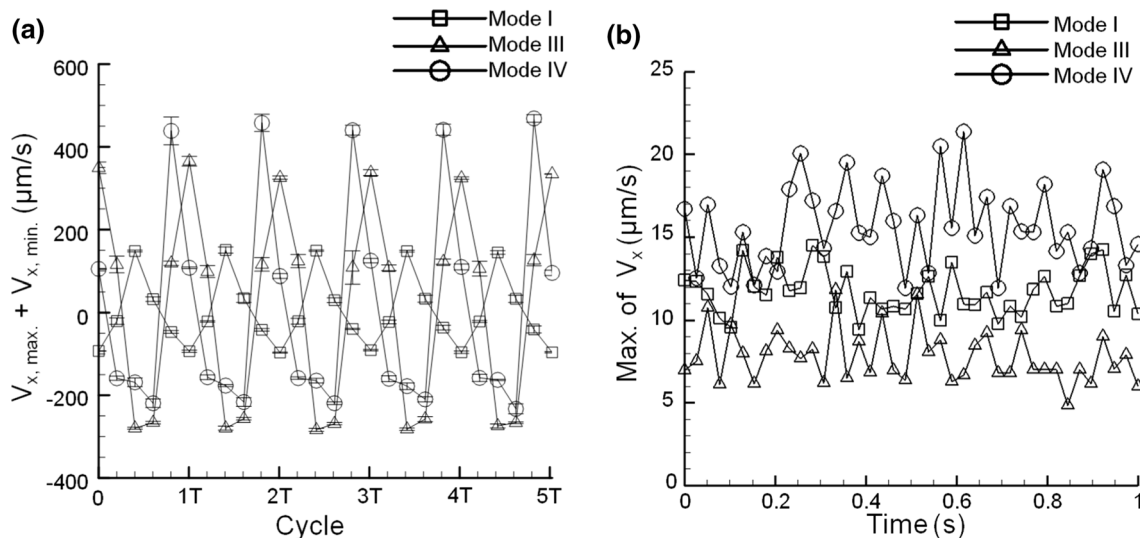

Fig. 5 The effect of artificial cilia distribution inside the microchannel quantified using µPIV at the frame rates of 200 Hz (**a**) and 40 Hz (**b**). Artificial cilia are rotated by following a circular trajectory at a rotational rate of 40 Hz. *Error bar* shows one standard deviation of the measured results over three cycles

also has substantial flow oscillations. Therefore, Mode I was selected as an ideal artificial cilia distribution given that considerable net flow could be generated along with significantly limited flow fluctuations.

3.3 Peak forward and backward flows

To provide the quantitative results of the amount of flow that can be generated during the effective and recovery strokes, which are critical in enhancing the net flow generation, time-ensembling induced flows at the selected cyclic time points of 0 and 0.5 T are shown in Fig. 6. Figure 6a shows the relative positions of the two selected time points with respect to the circular trajectory of each artificial cilium. The calculated net forward flow is largest with the Mode IV distribution at apeak velocity of 485.6 μm/s, whereas Mode I has the lowest peak velocity at 204.7 μm/s. Figure 6c shows that consistent results can be determined in the net backward flow comparison. These results indicated that the circulating nature of the artificial cilia actuation resulted in a considerably high forward flow followed by substantially high backward flow, thereby leading to significant flow fluctuations. Therefore, to reduce the degree of flow fluctuations, the triangular beating pattern of artificial cilia was specifically designed based on the results provided in the following section.

3.4 Induced flow field comparison between circular and triangular beating patterns

The triangular beating pattern was followed to reduce the effect of flow fluctuations during the artificial cilia

actuation. Figure 7 shows that the generated cyclic flow velocity over time was compared with that of the typical circular beating pattern. The concept of this action was based on a hydrodynamic benefit because the triangular beating pattern occurs during the artificial cilia actuation. The flat linear side of the triangular pattern, which is considerably close and parallel to the microchannel sidewall, is followed by the artificial cilia in the recovery stroke. This near-wall moving trajectory of the artificial cilia is expected to limit the amount of flow that is brought back, thereby significantly improving the net flow generation. Figure 7a shows that the peak backward velocity induced by the triangular path approaches −61.9 μm/s, which is much smaller than that induced by the circular path in terms of absolute value (with the peak backward velocity of −99.3 μm/s). In addition, the low back flow encountered using the triangular beating pattern of the artificial cilia actuation comes with a superior net flow velocity generation compared with the induced flow velocity by the circular beating pattern, as shown in Fig. 7b. The peak net flow induced by the triangular path can reach as high as 30.3 μm/s, which is twice larger than that induced by the circular path (14.5 μm/s). Moreover, upon comparison with other existing artificial cilia based microfluidic devices, it was found that the performance of the proposed microfluidic device with triangular beating pattern is superior in terms of flow generation. For instance, Wang et al. (2015) proposed a magnetically actuated artificial cilia based microfluidic device where the artificial cilia actuated in a tilted circular manner (Wang et al. 2015). Theoretically and experimentally they observed that with an optimal frequency setting, the device can generate an average flow speed of 70 and 5 μm/s for
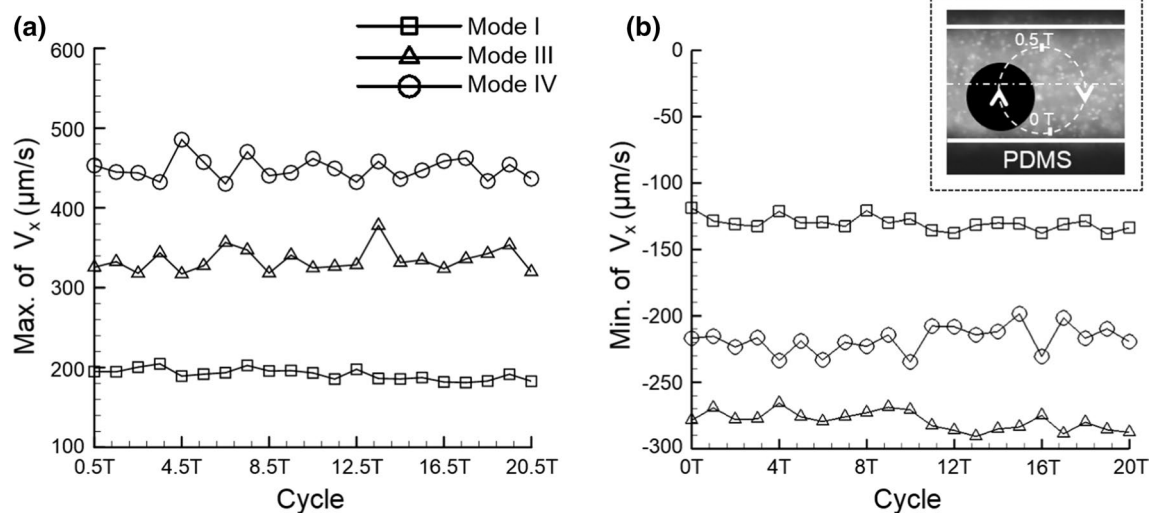

Fig. 6 Quantification of the peak forward and backward flows during the cyclic periods of the artificial cilia actuation in the three selected modes of artificial cilia distribution. **a** Calculated net forward flows at

0.5 T in each cycle. **b** Calculated net backward flows at 0 T in each cycle. *Inset picture* illustrates the peak forward flow at time point 0.5 T and the peak backward flow at 0 T in each cycle
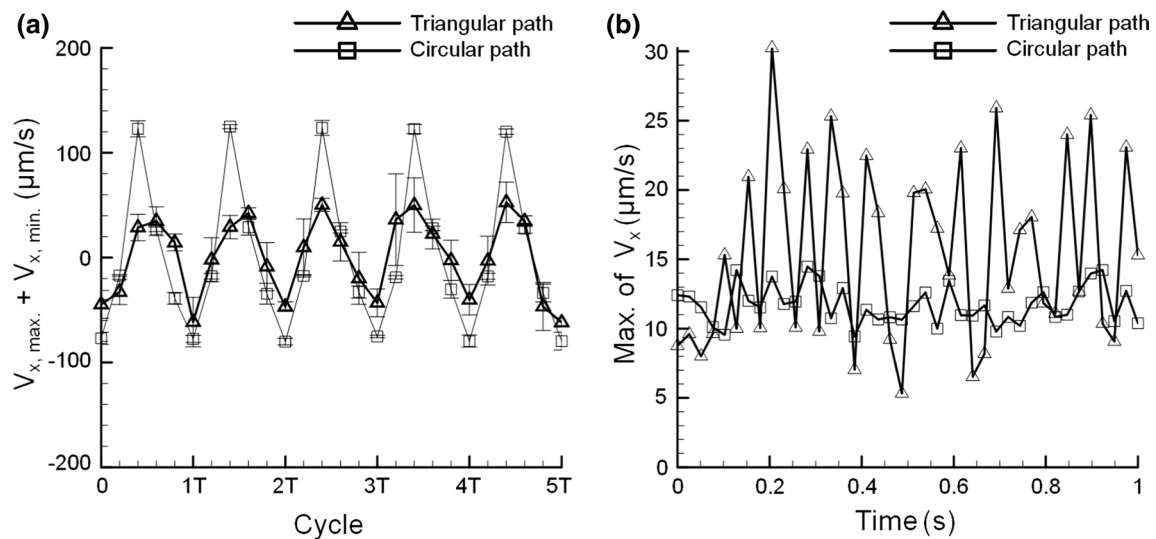
Fig. 7 Generated flow velocity with two beating patterns including the circular and triangular beating patterns using the recording rates of 200 Hz (**a**) and 40 Hz (**b**). *Error bar* shows one standard deviation of the measured results over three cycles

the working fluid of water and glycerol. Notice that the width of the microchannel and the population density of artificial cilia distribution is much larger than our device where a single array of artificial cilia was used inside the confinement of the channel. Similarly, other proposed artificial cilia based micro fluidic device where the authors reported simultaneous micromixing and micropropulsion can approximately generate an average flow velocity of 8 μm/s (Shields et al. 2010). In both the aforementioned case the artificial cilia were actuated in a circular manner where the backflow is inevitably significant. The flow generation through our proposed microfluidic device is par excellent compared to its existing counterparts due to the modified artificial cilia beating pattern. In addition, the scanning areas of the circular and triangular beating patterns are 3875 and 3778 μm², respectively. These results are comparable in terms of the energy budget necessary to generate these patterns. Through an improved control of beating patterns of artificial cilia, the flow propulsion efficiency can be elevated and even doubled. This concept can be further applied to investigate an optimal path for the beating behavior of the artificial cilia during the effective stroke by considering the hydrodynamic benefit.

4 Conclusions

The configuration of the confined microchannel with a single row of artificial cilia embedded for flow propulsion was investigated in a systematic manner. The design used the flow visualization method in conjunction with a series of image process algorithms to identify the key factor that contributed to the net flow generation on a microfluidic platform. In this study, the triangular beating pattern was initiated accordingly with the capability to reduce the amount of back flow generation compared with the typical circular one. Moreover, with this novel asymmetric beating pattern, the dependency of the net flow generation of artificial cilia based device towards the cilia position can be diminished. This finding is advantageous for biomedical-related applications, where accurate fluid control is necessary. In addition, the presented flow dynamic results and the employed analytical paradigm can assist the development of a new fluidic assessment tool to advance the current designs of microfluidics.

References

Abhari F, Jaafar H, Yunus NAM (2012) A comprehensive study of micropumps technologies. Int J Electrochem Sci 7:9765–9780

Belardi J, Schorr N, Prucker O, Ruhe J (2011) Artificial Cilia: generation of magnetic actuators in microfluidic systems. Adv Funct Mater 21:3314–3320

Chen CY, Chen CY, Lin CY, Hu YT (2013) Magnetically actuated artificial cilia for optimum mixing performance in microfluidics. Lab Chip 13:2834–2839

Chen CY, Yao CY, Lin CY, Hung SH (2014) Real-time remote control of artificial cilia actuation using fingertip drawing for efficient micromixing. J Lab Autom 19:492–497

Chen CY, Cheng LY, Hsu CC, Mani K (2015) Microscale flow propulsion through bioinspired and magnetically actuated artificial cilia. Biomicrofluidics 9:034105

Den Toonder J et al (2008) Artificial cilia for active micro-fluidic mixing. Lab Chip 8:533–541

Dorin A, Martin J (1994) A model of protozoan movement for artificial life. In: Gigante M, Kunni TL (eds) Proceedings computer graphics international 94. World Scientific, Melbourne, p 11

Evans BA, Shields AR, Carroll RL, Washburn S, Falvo MR, Superfine R (2007) Magnetically actuated nanorod arrays as biomimetic cilia. Nano Lett 7:1428–1434

Gauger EM, Downton MT, Stark H (2009) Fluid transport at low Reynolds number with magnetically actuated artificial cilia. Eur Phys J E Soft Mater 28:231–242

Laser DJ, Santiago JG (2004) A review of micropumps. J Micromech Microeng 14:R35–R64

Onck PR et al (2011) Magnetically-actuated artificial cilia for microfluidic propulsion. Lab Chip 11:2002–2010

Purcell EM (1977) Life at low reynolds-number. Am J Phys 45:3–11

Shields AR, Fiser BL, Evans BA, Falvo MR, Washburn S, Superfine R (2010) Biomimetic cilia arrays generate simultaneous pumping and mixing regimes. Proc Natl Acad Sci USA 107:15670–15675

Toonder JMJD, Onck PR (2013) Microfluidic manipulation with artificial/bioinspired cilia. Trends Biotechnol 31:85–91

Van den Beld WT, Cadena NL, Bomer J, de Weerd EL, Abelmann L, van den Berg A, Eijkel JC (2015) Bidirectional microfluidic pumping using an array of magnetic Janus microspheres rotating around magnetic disks. Lab Chip 15:2872–2878

Van Oosten CL, Bastiaansen CWM, Broer DJ (2009) Printed artificial cilia from liquid-crystal network actuators modularly driven by light. Nat Mater 8:677–682

Vilfan M, Potocnik A, Kavcic B, Osterman N, Poberaj I, Vilfan A, Babic D (2010) Self-assembled artificial cilia. Proc Natl Acad Sci USA 107:1844–1847

Wang Y, Gao Y, Wyss HM, Anderson PD, den Toonder JM (2015) Artificial cilia fabricated using magnetic fiber drawing generate substantial fluid flow. Microfluid Nanofluidics 18:167–174